

HORIZONTAL-BRANCH MORPHOLOGY AND THE PHOTOMETRIC EVOLUTION OF OLD STELLAR POPULATIONS

HYUN-CHUL LEE¹ AND YOUNG-WOOK LEE

Center for Space Astrophysics, Yonsei University, Shinchon 134, Seoul 120-749, Korea

AND

BRAD K. GIBSON

Centre for Astrophysics and Supercomputing, Swinburne University, Mail Number 31, P.O. Box 218, Hawthorn, VIC 3122, Australia

Received 2002 May 21; accepted 2002 August 1

ABSTRACT

Theoretical integrated broadband colors ranging from far-UV to near-IR have been computed for old stellar systems from our evolutionary population synthesis code. These models take into account, for the first time, the detailed systematic variation of horizontal-branch (HB) morphology with age and metallicity. Our models show that some temperature-sensitive color indices are significantly affected by the presence of blue HB stars. In particular, $B-V$ does not become monotonically redder as metallicity increases at given ages, but becomes bluer by as much as ~ 0.15 mag because of the contribution from blue HB stars. Similar trends are also found in the Washington photometric system. In addition to appropriate age-sensitive spectrophotometric indices, the use of far-UV to optical colors is proposed as a powerful age diagnostic for old stellar systems with differing HB morphologies. Our models are calibrated in the $B-V$, $V-I$, $C-T_1$, and $M-T_1$ versus $[\text{Fe}/\text{H}]$ planes, using low-reddened Galactic globular clusters (GCs) [$E(B-V) < 0.2$], and the relative age difference between the older inner halo Galactic GCs and younger outer halo counterparts is well reproduced. Several empirical linear color-metallicity transformation relations are assessed with our models, and it is noted that they may not be safely used to estimate metallicity if there are sizable age differences among GCs within and between galaxies. M31 GCs are found to be fundamentally similar to those in the Milky Way, not only in the optical to near-IR range, but also in the UV range. For globular cluster systems in two nearby giant ellipticals, M87 and NGC 1399, the current available photometric data in the literature do not appear sufficient to provide robust age discrimination. It is anticipated, however, that the detailed population models presented here, coupled with further precise spectrophotometric observations of globular cluster systems in external galaxies from the large ground-based telescopes and space UV facilities, will enable us to accurately estimate their ages and metallicities.

Key words: galaxies: formation — galaxies: star clusters — stars: horizontal-branch

On-line material: color figures

1. INTRODUCTION

When stellar systems can be resolved into individual stars, such as open and globular star clusters in the Milky Way and Local Group galaxies, one can derive their ages and metallicities via isochrone fitting to the main-sequence turn-off and red giant branch in the color-magnitude diagram and fitting luminosity functions to the white dwarf cooling sequence (Hansen et al. 2002). This luxury does not exist for more distant systems, however, so one must rely upon their integrated colors or spectra. Calibrating theoretical spectrophotometric quantities using local, resolved systems is then surely a necessary step (e.g., Gibson et al. 1999).

Since local and nearby extragalactic globular clusters (GCs) are easily detected and feasible for analysis because of their rather simple nature, there have been many photometric studies of globular cluster systems in external galaxies that have revealed important information regarding the link between GC systems and their host galaxies (see Ashman & Zepf 1998 for a recent review). Information regarding their relative ages within a given galaxy or between galaxies is particularly relevant

for studying the hierarchical formation of galaxies. As globular cluster ages and metallicities become better constrained, the opportunities for understanding the process of galaxy formation and its subsequent evolution can only increase.

In recent years, there have been many efforts to develop evolutionary population synthesis models (e.g., Bruzual & Charlot 1993; Worthey 1994, hereafter W94; Buzzoni 1995; Vazdekis et al. 1996; Maraston 1998; Lee 2001a, 2001b) in order to analyze the integrated spectrophotometric quantities from globular clusters and galaxies and to derive their mean ages and metallicities. It is true that those integrated quantities are indeed determined by the age and metallicity of those stellar systems, but it should also be kept in mind that they are the two most arguably dominant parameters that determine globular clusters' horizontal-branch (HB) morphologies. Therefore, the integrated colors of GCs should be affected to some degree by differing HB morphologies at the similar metallicity (the "second parameter" effect). It is now generally accepted that age is the *global* second parameter that controls HB morphology (after the first parameter, metallicity: Lee, Demarque, & Zinn 1994; Sarajedini, Chaboyer, & Demarque 1997; Salaris & Weiss 2002), although for some GCs a third (or more) parameter may be needed to explain their peculiar HB morphologies (such as blue tail phenomenon, Recio-Blanco et al. 2002).

¹ Current address: Centre for Astrophysics and Supercomputing, Swinburne University, Mail Number 31, P.O. Box 218, Hawthorn, VIC 3122, Australia.

We are extending this second-parameter analysis to broader age ranges in this work, which is applicable even to potentially older stellar systems than we have in the Milky Way, and investigate how variation of HB morphology influences the integrated photometric quantities. With a better understanding of post-main-sequence stellar evolution, it is now feasible to study the systematic effects of those evolved stars on the integrated spectrophotometric values. One vivid example has already appeared in Lee, Yoon, & Lee (2000; hereafter Paper I) for the realistic assessment of ages of old stellar systems using the $H\beta$ index. A unique aspect of these models lies in their treatment of the systematic variation of HB morphology as a function of age and metallicity. In this paper we present a detailed quantitative analysis of the effects of HB morphology on theoretical integrated broadband colors ranging from far-UV to near-IR at various stages of age and metallicity. In addition, integrated broadband colors that have been used to estimate the metallicity of globular clusters are examined with our models in order to check the veracity of the so-called color-metallicity transformation relations that are widely used but based solely upon Galactic GCs.

In § 2 our population models, developed with and without consideration of HB stars, are presented and compared with those of other groups. We first consider optical to near-IR colors, including those using the Washington photometric system, an investigation of UV to optical colors is then presented. Section 3 corroborates the validity of our models with HB stars by calibrating them using a sample of relatively low-reddened Galactic GCs, and our results are then used to assess several color-metallicity transformation relations. We compare our models with available UV to near-IR data for GC systems in M31, M87, and NGC 1399 (e.g., Cohen, Blakeslee, & Ryzhov 1998; Kissler-Patig et al. 1998, hereafter KBSFGH98; Forbes et al. 2001a). In most cases we have specially sought age-sensitive colors to combine with spectroscopic metallicity information. A discussion of the implications of our work is provided in § 4.

2. POPULATION MODELS OF INTEGRATED BROADBAND COLORS WITH AND WITHOUT HORIZONTAL-BRANCH STARS

The present models were constructed, in essence, from the same evolutionary population synthesis code developed to study the stellar populations of globular clusters (Paper I). In summary, we have used the Yale isochrones (Demarque et al. 1996) rescaled for α -element enhancement² (Salaris, Chieffi, & Straniero 1993) and the HB evolutionary tracks by Yi, Demarque, & Kim (1997). For metal-rich ($[Fe/H] > -0.5$) populations the value of the helium enrichment parameter, $\Delta Y/\Delta Z = 2$, was assumed. The standard Salpeter (1955) initial mass function was adopted for calculating the relative number of stars along the isochrones. For the conversion from theoretical quantities to observable quantities we employed the stellar library of Lejeune, Cuisinier, & Buser (1997, 1998) in order to cover the largest possible range in stellar parameters, such as metallicity,

temperature, and gravity. As discussed in Paper I, we have rescaled the isochrone ages such that the 15 Gyr isochrones now correspond to present-day 12 Gyr old populations³ and $\Delta t = 0$ corresponds to $t \simeq 12$ Gyr.

The treatment of the detailed systematic HB morphology variation with age and metallicity is also compatible with that of Paper I. Figure 1 presents our model isochrones as a function of HB morphology $[(B-R)/(B+V+R)]$, where B , V , and R are the numbers of blue HB stars, RR Lyrae variables, and red HB stars, respectively; Lee et al. 1994] and metallicity $[Fe/H]$. The Galactic GC data of Lee et al. (1994) are overplotted. For NGC 4590 and NGC 6656 the updated HB types are adopted from the Harris (1996, 1999 June version) compilation. In order to match the observed HB morphology of inner halo Galactic GCs (Galactocentric radius ≤ 8 kpc) at their currently favored mean age (~ 12 Gyr, $\Delta t = 0$ Gyr) in light of the distance scale suggested by

³ According to Fig. 14 and Table 7 of Yi et al. (2001), it is assured that our treatment of age reduction effect by 3 Gyr is basically correct, though a conundrum remains, as the trend may be reversed in the metal-rich regime.

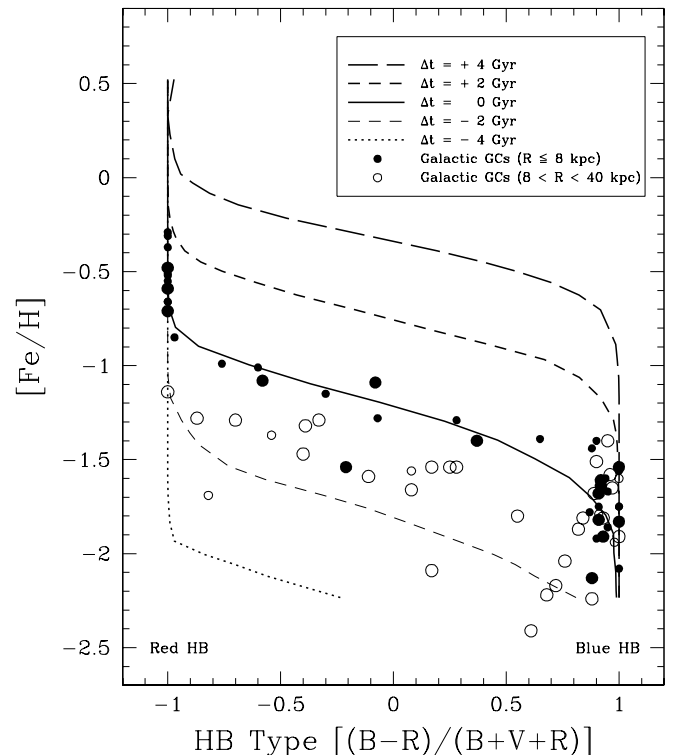


Fig. 1.—Detailed systematic HB morphology variation established by matching the tight correlations between the HB morphology type and $[Fe/H]$ of the inner halo Galactic globular clusters (Galactocentric distance ≤ 8 kpc; filled symbols) at their currently favored mean age (~ 12 Gyr, $\Delta t = 0$ Gyr; solid line). Open symbols represent the outer halo Galactic GCs. The dotted line and the short-dashed line (thinner line) represent the predicted model relationship for populations that are 4 and 2 Gyr younger, and the short-dashed (thicker line) and long-dashed lines represent that for populations that are 2 and 4 Gyr older than the inner halo Galactic GCs, respectively. The larger symbols are the relatively low-reddened Galactic GCs $[E(B-V) < 0.2]$ that are plotted in Fig. 7. Note that the inner halo Galactic GCs are not only systematically older, but also more tightly grouped along our model isochrone than those in the outer halo in this diagram (see text). Data are from Lee et al. (1994).

² The value $[\alpha/Fe] = 0.4$ for $[Fe/H] < -1.3$; $[\alpha/Fe]$ goes from 0.4 to 0.0 as $[Fe/H]$ goes from -1.3 to 0.0, and $[\alpha/Fe] = 0.0$ for $[Fe/H] > 0.0$ (Wheeler, Sneden, & Truran 1989).

Hipparcos (e.g., Chaboyer et al. 1998), the value of η , the parameter in Reimers (1975) law, was taken to be $\eta = 0.65$. We then investigate the age range $-4 \text{ Gyr} \leq \Delta t \leq +4 \text{ Gyr}$. In Figure 1 the larger symbols are the relatively low-reddened Galactic GCs [$E(B-V) < 0.2$] that will be used to calibrate our models in § 3.1. It is useful to note here that the inner halo Galactic GCs (*filled circles*) are not only systematically older, but also more tightly grouped along our model⁴ isochrone than those in the outer halo (*open circles*).

We have not taken into account the effects of extended blue tails on the HB, or blue stragglers, in this work, as it remains difficult to quantify them systematically with age and metallicity. We recognize, though, that some UV indices and colors may be affected by their inclusion. Furthermore, except for the case of UV to optical colors, post-asymptotic giant branch (PAGB) stars are not considered here.

⁴ The filled symbol that lies significantly away from the inner halo locus in Fig. 1 is NGC 6584. According to Table 5 of Dinescu, Girard, & van Altena (1999), NGC 6584 is of very much eccentric orbital parameters ($R_a \sim 13 \text{ kpc}$, $R_p \sim 1 \text{ kpc}$), and therefore it may not belong to the true inner halo cluster category (see also § 4 of Lee et al. 1994 for a more detailed description). Actually, taking NGC 6584 as an outer halo cluster could make our assertion stronger.

2.1. Optical to Near-IR Range Colors

Here we address the theoretical integrated broadband colors in the standard *UBVR*K filter system. The following is a brief summary of the computational procedure. First, for each star (or group of stars, after binning) with a given metallicity, temperature, and gravity we find the corresponding colors and the bolometric correction values from the color tables of Lejeune et al. (1998). Second, these are converted into each bandpass' luminosity. Finally, after each bandpass's luminosity has been summed, for a simple stellar population of a given metallicity and age we compute the integrated photometric magnitudes for each bandpass. Integrated broadband colors are then calculated from these computed magnitudes.

Figure 2 presents our theoretical predictions for the integrated broadband colors: (a) $U-V$; (b) $B-V$; (c) $V-I$; and (d) $V-K$ as a function of $[\text{Fe}/\text{H}]$. We find that our models with HB stars (*thick lines*) show quantifiable differences from those without HB stars (*thin lines*), notably in Figure 2b. *Because of the contribution from blue HB stars, $B-V$ does not become monotonically redder as metallicity increases at given ages, but becomes bluer by as much as $\sim 0.15 \text{ mag}$. Similar "wavy" features⁵ have been seen in the temperature-*

⁵ Selected synthetic CMDs in Fig. 5 of Lee et al. (2000) would be helpful for understanding these "wavy" features.

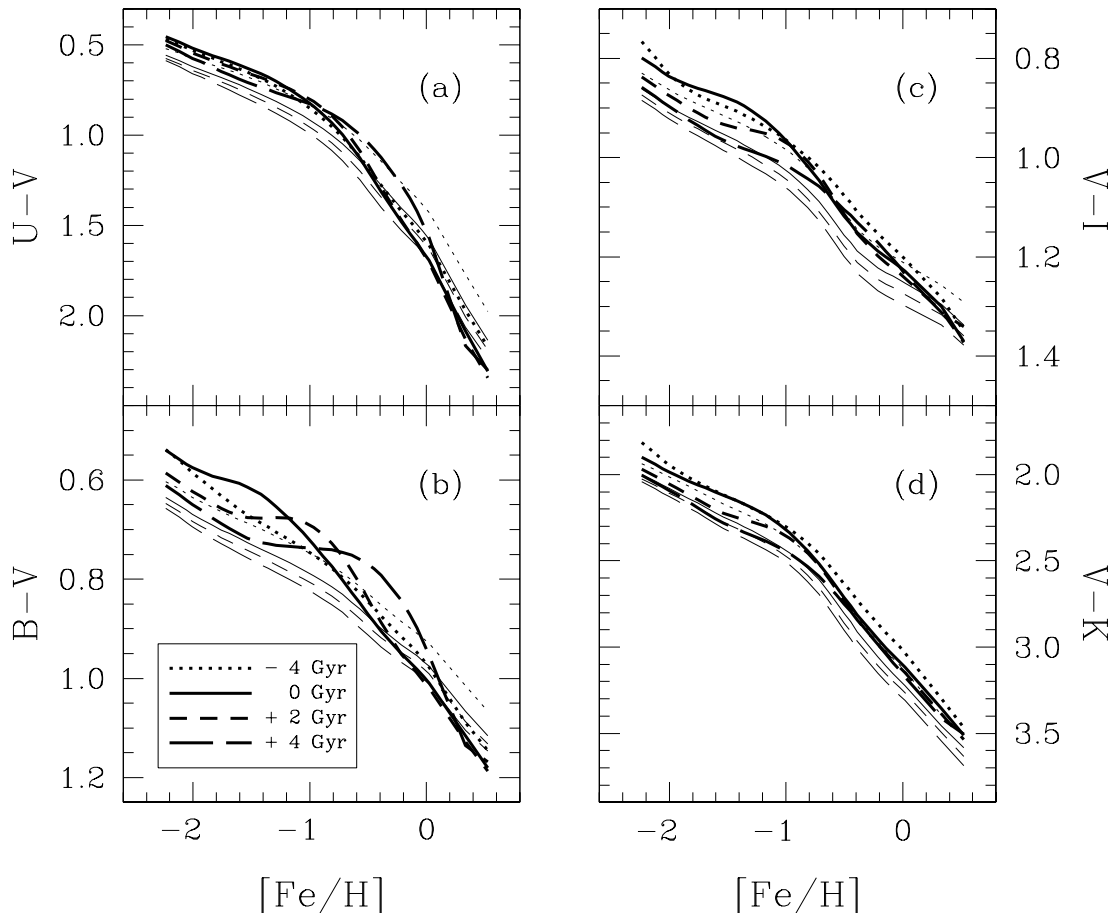


FIG. 2.—Effects of HB stars on (a) $U-V$, (b) $B-V$, (c) $V-I$, and (d) $V-K$ colors as predicted from our models (see text). The colors are plotted against $[\text{Fe}/\text{H}]$ for four relative ages ($\Delta t = -4, 0, +2$, and $+4 \text{ Gyr}$, respectively). Thin lines represent models without HB stars, while thick lines represent those with HB stars based on the model loci of Fig. 1. Note that $B-V$ colors are particularly affected by blue HB stars and become bluer by $\sim 0.15 \text{ mag}$ than the models without HB stars similar to the feature seen in the $H\beta$ index (Paper I).

sensitive $H\beta$ index (Paper I). Other colors appear to be affected to some degree by our treatment of HB morphology variations, but the effects are not as prominent in the age range investigated here. In the succeeding investigation we will mainly concentrate on $B-V$ and $V-I$, because these two colors are two of the most frequently referred to in the literature.

There have been related studies of the theoretical integrated broadband colors in recent years (e.g., W94; Kurth, Fritze-von Alvensleben, & Fricke 1999, hereafter KFF99; Brocato et al. 2000, hereafter BCPR00), however, the different stellar physics and calibrations result in inevitable differences in their predictions. In particular, the different treatment of the HB is noteworthy and may result in significant differences in the models. For instance, W94 treated HB stars as a rather simple red clump, providing results similar to those of our models without HB stars.⁶ Both KFF99 and BCPR00 include HB stars in their models but their values of η , the efficiency of mass loss, are different ($\eta = 0.35$ in KFF99 and $\eta = 0.4$ in BCPR00) from ours ($\eta = 0.65$), probably because they adopted ~ 15 Gyr for the absolute age of Galactic GCs (see Table 1 of Yi et al. 1999 for the different choice of η in connection with that of the absolute age of Galactic GCs). For example, Figure 3 shows significantly different HB morphologies at the same metallicity and simi-

lar age as different values of η (different amounts of mass loss) are adopted. The Padua isochrones (Girardi et al. 2000) employ the smaller value of $\eta = 0.4$, compared with that which we use in this study (*open circles and small points*)⁷, and seemingly no mass dispersion is taken into account (*triangles*). In combination, these issues result in different model predictions, particularly for temperature-sensitive indices. BCPR00 tested several values of η and showed that higher values of η gave bluer colors (see their Fig. 8).

Despite these differences it is interesting to note that both KFF99 and BCPR00 do show slight crossovers among different ages at the low-metallicity region in the $B-V$ versus $[Fe/H]$ plane (see Fig. 3 of KFF99 and Fig. 9 of BCPR00). In addition, it is noted that almost all models reveal some nonlinear feature in the $V-I$ versus $[Fe/H]$ plane, being flatter in the low-metallicity range, $[Fe/H] < -1.0$. The importance of this nonlinearity will be addressed further in § 3.1 when the empirical *linear* color-metallicity relations are assessed with our models.

2.2. Washington Photometric System

The Washington photometric system introduced by Cantina (1976) was originally developed as an optimum system for deriving temperatures (T_1 and T_2 filters) and abundances (C and M filters) for late-type giant stars. In essence, the C filter covers about two-thirds of the U and B filter, and the M filter has its peak between the B and V filters and covers about half of each filter. The T_1 and T_2 filters are almost identical to the R and I filters, respectively (see Fig. 1 of Lejeune & Buser 1996). Because of its efficiency with the broader bandpasses than the commonly used $UBVRI$, the popularity of this system has grown in recent years for obtaining integrated colors of GC systems in distant galaxies (e.g., Geisler & Forte 1990, hereafter GF90; Lee & Geisler 1993, hereafter LG93; Secker et al. 1995; Zepf, Ashman, & Geisler 1995; Ostrov, Forte, & Geisler 1998). Perhaps the most important use of this system is in the determination of metallicities for distant GCs from their integrated colors, especially ($C-T_1$), with its very long color baseline (GF90).

Although the number of observational studies using the Washington photometry has been increasing, little has yet been done in modeling the colors for the system, at least in comparison with the extant body of model colors for the $UBVRI$ system. In this context we investigate the theoretical integrated colors using the Washington photometric system. The computation of integrated colors using the Washington system required some modifications to the procedure described in § 2.1. First, we generate the integrated spectral energy distributions (SEDs) for a simple stellar population of a given metallicity and age using the flux tables (Lejeune et al. 1998). Then the fluxes within each bandpass of the Washington photometric system are integrated using the relative filter response functions, and we calculate the integrated magnitudes and colors.⁸

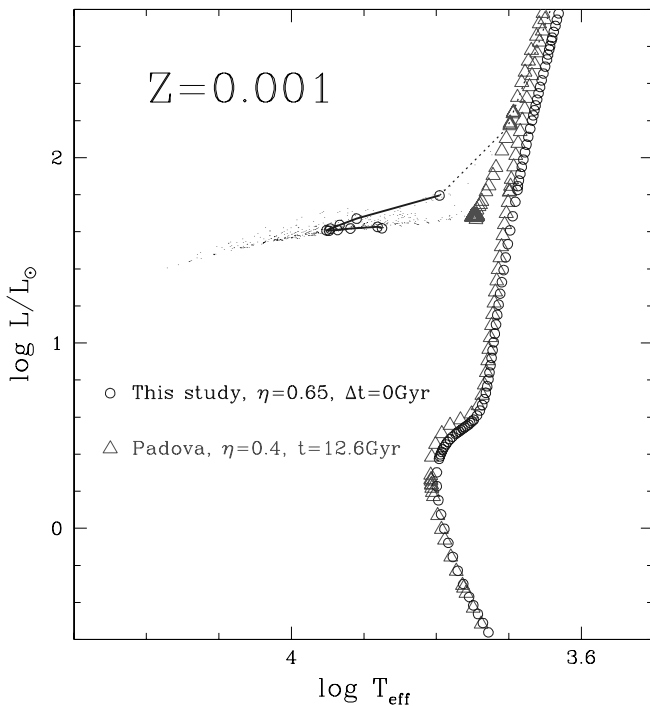


FIG. 3.—Selected HR diagram showing differences of this study's HB morphology (*open circles*) from the Padua isochrone's one (*triangles*) at the same metal abundance ($Z = 0.001$) and similar age. This takes place mainly because of adopting different amounts of mass loss (i.e., different values of η) and due to our treatment of mass dispersion (*small points*: realistic HB morphology with Gaussian mass dispersion for our case). Combination of these issues results in different model predictions, particularly for temperature-sensitive indices. The evolutionary track of our models' mean mass HB star is connected by lines (see text).

⁷ The solid line in Fig. 3 represents the HB evolutionary track and the dashed line does that of post-HB. For this study we present the case with HB stars only. The study with post-HB stars can be found in Lee (2001a).

⁸ We have taken the response functions of the Washington system from Kitt Peak National Observatory Web site, at <http://www.noao.edu/kpno>.

⁶ At <http://astro.wsu.edu/worthey>.

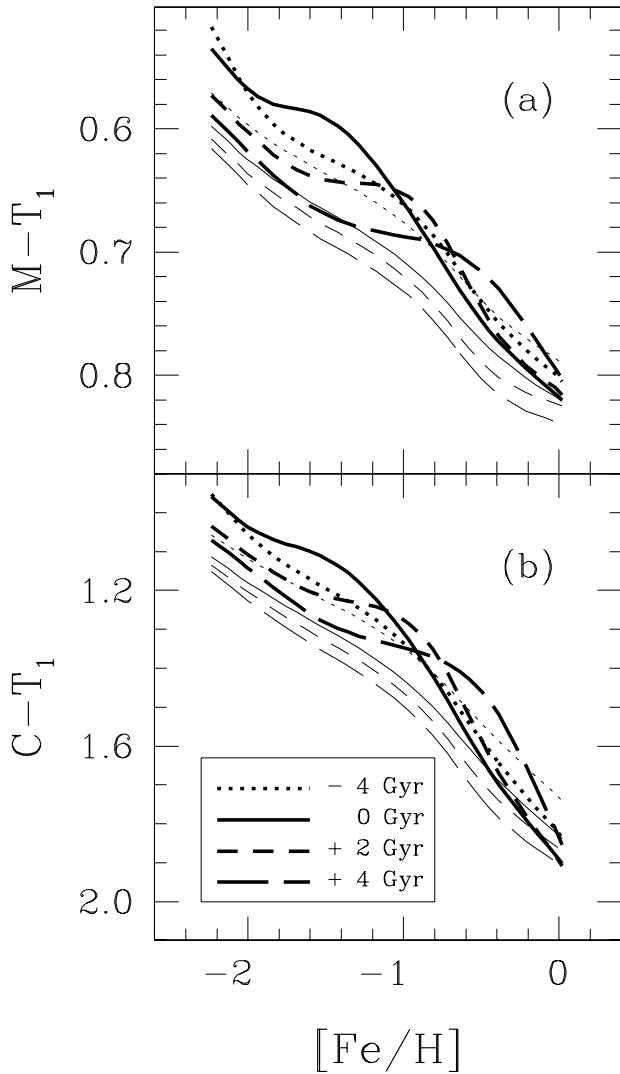


FIG. 4.—Effects of HB stars on (a) $M-T_1$ and (b) $C-T_1$ colors as predicted from our models. The colors are plotted against $[\text{Fe}/\text{H}]$ for four relative ages. Symbols are same as in Fig. 2. Note that both $M-T_1$ and $C-T_1$ colors are affected by blue HB stars and become bluer by ~ 0.08 mag and by ~ 0.2 mag, respectively, than the models without HB stars similar to the feature seen in Fig. 2b.

Figure 4 shows effects of HB stars on (a) $M-T_1$ and (b) $C-T_1$ colors, as predicted from our models, as a function of $[\text{Fe}/\text{H}]$. Thin lines represent models without HB stars, while thick lines include the effects of HB stars, based on the model loci of Figure 1. It is found that both $M-T_1$ and $C-T_1$ colors are affected by blue HB stars and become bluer by ~ 0.08 mag and by ~ 0.2 mag, respectively, than the models without HB stars, similar to the feature seen in Figure 2b ($B-V$) and the $H\beta$ index seen in Figure 6 of Paper I. Geisler, Lee, & Kim (1996) examined the age, HB morphology, and metallicity sensitivities of the integrated $C-T_1$ color, based on the work of Cellone & Forte (1996, hereafter CF96) and concluded that it was an efficient metal abundance index; in contrast, we have found that the integrated $C-T_1$ is, to some degree, affected by the systematic variation of HB morphology with age and metallicity. It is difficult to compare our results directly with those of CF96, because they give their outputs only at two given ages (5 and 15 Gyr) and

base their predictions upon the older Buzzoni (1989, 1995) population synthesis code. However, it is evident even in CF96 that the predicted $C-T_1$ with an intermediate HB morphology is bluer than that of a red HB at the same metallicity (see Fig. 7 of Geisler et al. 1996). Theoretical modeling of the Washington photometric system based on a large sample of individual stars would undoubtedly give more credibility to this particular aspect of stellar population synthesis work (e.g., Lejeune & Buser 1996).

2.3. UV to Optical Range Colors

The computational procedure for the relevant UV band-pass magnitudes is almost identical to that which we described in § 2.2. For the case of UV to optical colors of an old stellar population, however, the contribution from PAGB stars is considered. A small number of PAGB stars can have a significant impact upon the integrated UV flux. The PAGB contribution is somewhat stochastic by nature, due to small number statistics being driven primarily by their short lifetimes. For instance, the evolutionary lifetime of a $0.565 M_{\odot}$ PAGB star is only 40,000 yr (Schönberner 1983) compared with about 100 Myr for HB stars. We have quantified the expected number ratio of PAGB to HB stars, based on the ratio of their evolutionary lifetimes after more than 10 simulations, and added the corresponding averaged fluxes using Schönberner's (1983) evolutionary track for a $0.565 M_{\odot}$ PAGB star.

Figure 5 shows several integrated SEDs from our models, with and without PAGB stars. Three ages ($\Delta t = +4, 0,$ and -4 Gyr) are illustrated at the given metallicity ($[\text{Fe}/\text{H}] = -1.17$). All fluxes have been normalized to

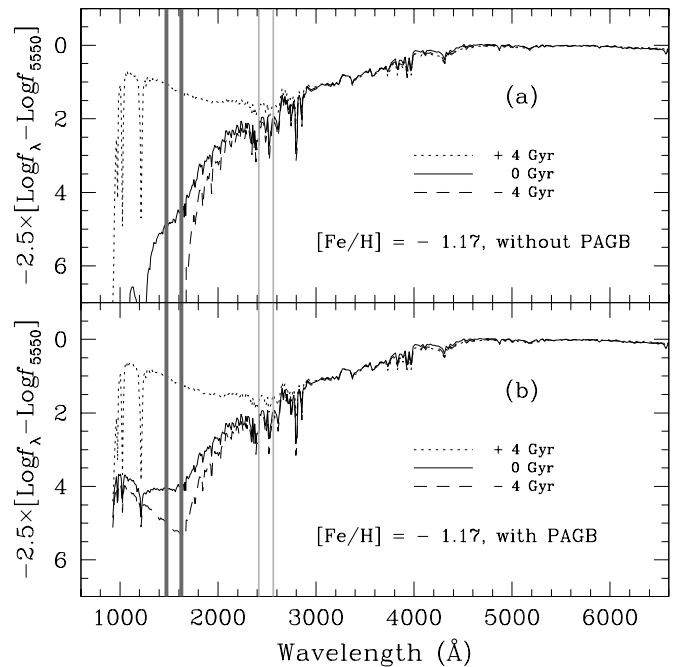


FIG. 5.—Selected integrated SEDs from our models (a) without and (b) with including contribution from PAGB stars drawn for three different ages ($\Delta t = +4, 0,$ and -4 Gyr, respectively) at a given metallicity ($[\text{Fe}/\text{H}] = -1.17$). The far-UV (thick gray column) and the near-UV (thin gray column) bandpasses that we have employed in this study are indicated. Note that once the old populations are fairly UV bright, especially in the far-UV range due to hot blue HB stars (dotted lines), the PAGB contribution becomes unimportant.

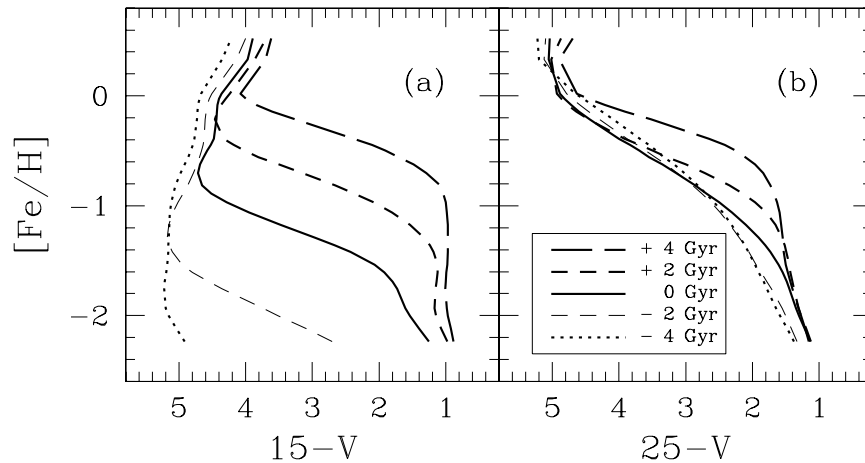


FIG. 6.—(a) $15-V$ and (b) $25-V$ colors from our models including contributions from PAGB stars are plotted as a function of $[\text{Fe}/\text{H}]$ for five relative ages. Symbols are same as in Fig. 1. Note that $15-V$ vs. $[\text{Fe}/\text{H}]$ plot is reminiscent of the HB type vs. $[\text{Fe}/\text{H}]$ plot drawn in Fig. 1.

unity at 5550 \AA and then converted into magnitudes. One can then easily estimate magnitude differences relative to the V band from Figure 5. For the ensuing investigation $15-V$ and $25-V$ are defined as the magnitude differences between the far-UV and the near-UV band centered at 1550 and 2490 \AA , respectively, with 150 \AA bandwidths, as indicated by the gray columns in Figure 5 and the visual band. The dashed lines in Figure 5 ($\Delta t = -4$ Gyr) show that old stellar systems with only red HB stars would have minimal far-UV flux without a PAGB contribution. From the dotted lines in Figure 5 ($\Delta t = +4$ Gyr), we can see that, once hot blue HB stars begin to become important for very old systems, the PAGB contribution becomes increasingly insignificant. Consequently, it is seen that the older populations with the bluer HB stars should be relatively UV bright, especially in the far-UV range. In the near-UV range, however, it is seen that the contribution from PAGB stars is relatively unimportant.

In Figure 6 $15-V$ and $25-V$ colors from our models, including contributions from PAGB stars, are plotted against $[\text{Fe}/\text{H}]$ for five relative ages ($\Delta t = -4, -2, 0, +2$, and $+4$ Gyr, respectively). The $15-V$ versus $[\text{Fe}/\text{H}]$ plot (Fig. 6a) is reminiscent of Figure 1, which suggests that the far-UV to optical colors also describe the HB morphology, in a manner similar to that of the optical to near-IR colors. This leads us to believe that far-UV photometry, in combination with optical data, will provide a useful age discriminant for GC systems. In Figure 6b, however, it is found that $25-V$ from our models is relatively insensitive to the variation of HB morphology, compared with $15-V$. This is because in the near-UV range the contribution from main-sequence turnoff stars is not insignificant. These models will be tested using the available UV data sets of Galactic and M31 GCs in § 3.3.

3. COMPARISON WITH OBSERVATIONS

3.1. Calibration via Globular Cluster System in the Milky Way

Having discussed the theoretical aspects of generating integrated broadband colors in § 2, we now provide an empirical calibration for the models using the Milky Way's GC system. We adopt Harris's (1996) data set for calibra-

tion purposes but restrict ourselves to those clusters with line-of-sight reddenings $E(B-V) < 0.2$. The more highly reddened clusters possess increasingly uncertain photometry. When needed, the extinction law of Cardelli, Clayton, & Mathis (1989) is adopted.

Figure 7 contrasts this sample of Galactic GCs (*filled circles*: inner halo clusters; *open circles*: outer halo clusters) with our models in (a) the $(B-V)_0$; (b) $(V-I)_0$; (c) $(M-T_1)_0$; and (d) $(C-T_1)_0$ versus $[\text{Fe}/\text{H}]$ planes. The integrated $B-V$ and $V-I$ colors of Galactic GCs have essentially negligible uncertainties, because of the intrinsic brightness of the sample; the largest uncertainties can be traced to the uncertainty in foreground reddening, which corresponds to less than 0.02 mag for this sample. The limited sample of Galactic GCs with Washington photometry (Harris & Cantnera 1977) is shown, along with our models, in Figures 7c and 7d. As a matter of fact, this is a first-ever try to separate the Milky Way globulars into subpopulations and to address their relative age differences using broadband colors. It appears that our models reproduce the differences between inner and outer halo clusters noted in Figure 1, in the sense that the inner halo clusters are not only more tightly grouped along the isochrone than the outer halo counterparts, but also relatively older from the eye fit.

In Figure 7 we applied $0.03, 0.01$, and 0.05 mag zero-point offsets to the models in $B-V$, $M-T_1$, and $C-T_1$, respectively, in order to minimize the residuals between the models and the data. These offsets may arise from uncertainties in the adopted theoretical stellar atmospheres or our rough age reduction treatment by 3 Gyr or the color-effective temperature calibration (e.g., Girardi 2001; Kurucz 2001; Yi et al. 2001; Westera et al. 2002). We apply the same offsets for the comparison against extragalactic systems in § 3.2. The models of Figure 7 support the hypothesis that the realistic HB morphology inclusion is truly important, and the fact that even the small relative age difference between inner and outer halo clusters is rather satisfactorily reproduced indicates that we are making some progress here over the previous attempts (e.g., Fig. 43 of W94, Figs. 3 and 4 of KFF99, Figs. 6 and 9 of BCPR00, and Fig. 7 of Geisler et al. 1996).

Before our models are applied to extragalactic GC systems, several empirical *linear* color-metallicity trans-

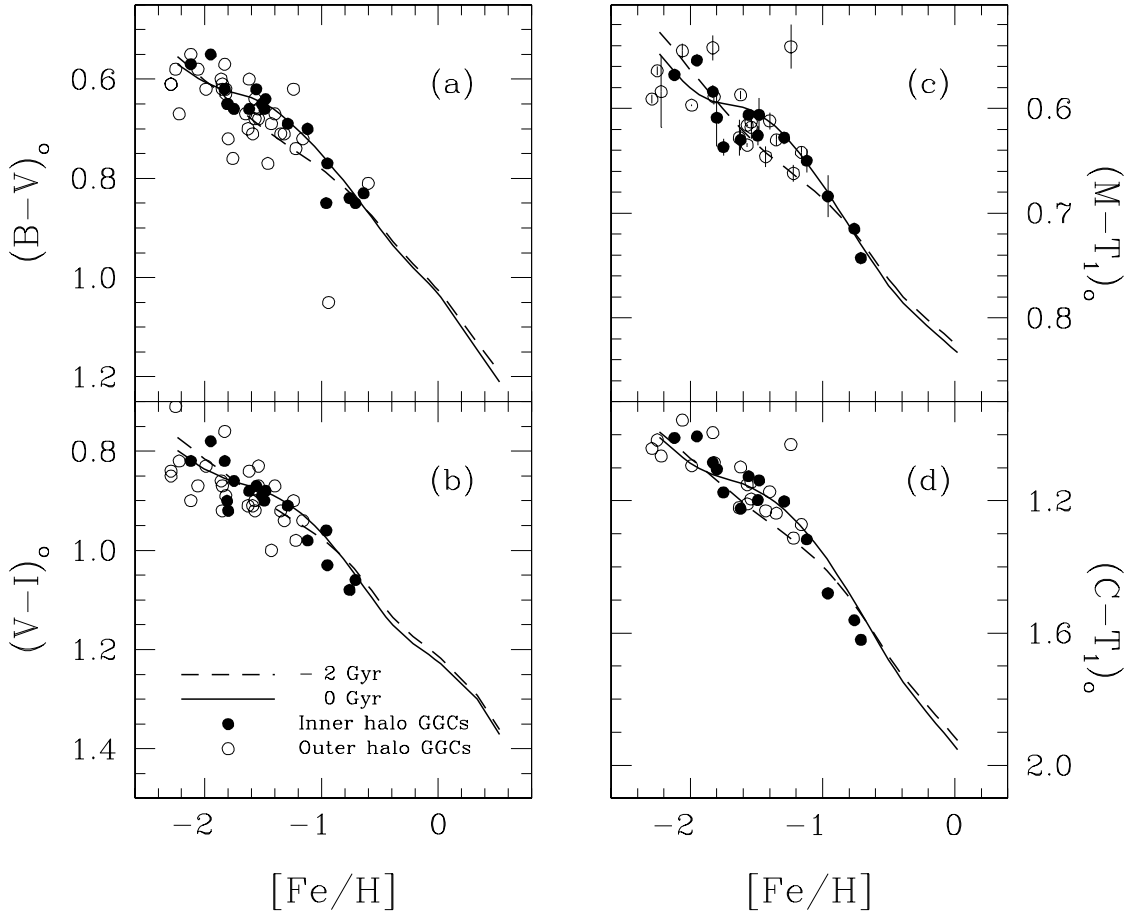


FIG. 7.—Relatively low-reddened Galactic GCs [$E(B-V) < 0.2$; filled circles: inner halo clusters; open circles: outer halo clusters] used to calibrate our models in the (a) $(B-V)_0$, (b) $(V-I)_0$, (c) $(M-T_1)_0$, and (d) $(C-T_1)_0$ vs. $[\text{Fe}/\text{H}]$ planes. Note that our models not only represent the observational data reasonably well but also reproduce the different trends, particularly in terms of the relative ages, between inner and outer halo clusters noted in Fig. 1. In $B-V$, $M-T_1$, and $C-T_1$, 0.03 mag, 0.01 mag, and 0.05 mag zero-point offsets were applied, respectively (see text).

formation relations in the literature were assessed (see Fig. 8). First, in the $[\text{Fe}/\text{H}]$ versus $(B-V)_0$ plane (Fig. 8a), Couture, Harris, & Allwright’s (1990, hereafter CHA90) relation is shown with our models, $(B-V)_0 = 0.200[\text{Fe}/\text{H}] + 0.971$. The CHA90 relation is based on Galactic GCs with $E(B-V) \leq 0.4$. Figure 8b shows the $[\text{Fe}/\text{H}]$ versus $(V-I)_0$ plane, with CHA90’s relation, $[(V-I)_0 = 0.198[\text{Fe}/\text{H}] + 1.207]$, KBSFGH98’s relation, $[[\text{Fe}/\text{H}] = -4.50 + 3.27(V-I)]$, Kundu & Whitmore’s (1998, hereafter KW98) relation, $[[\text{Fe}/\text{H}] = -5.89 + 4.72(V-I)]$, and Harris et al.’s (2000, hereafter HKHHP00) relation, $[(V-I)_0 = 0.17[\text{Fe}/\text{H}] + 1.15]$, contrasted with our models. These latter relations are also made using the relatively low-reddened Galactic GCs, except that of KBSFGH98, who made their relation using the NGC 1399 GCs (see § 3.2). The $[\text{Fe}/\text{H}]$ versus $(C-T_1)_0$ plane is shown in Figure 8c, with GF90’s relation, $[[\text{Fe}/\text{H}] = 2.35(C-T_1)_0 - 4.39]$, compared with our models. GF90’s relation is based upon the data set of Harris & Cantenna (1977), using the Galactic GCs in the range $-2.25 \leq [\text{Fe}/\text{H}] \leq -0.25$.

Because these color-metallicity transformation relations rely upon Galactic GCs in a limited range of color [$0.6 < (V-I)_0 < 1.1$], caution must be employed when extrapolating their use beyond this range (e.g., Harris et al. 1992; Harris, Harris, & McLaughlin 1998). Our models in

Figure 8 suggest that $B-V$ may not be a good metallicity indicator and even $V-I$ should be used with extra caution in deriving metallicity because of the model nonlinearity. GF90 demonstrated that the $C-T_1$ index is highly metallicity sensitive, with a total range of 0.84 mag for the Galactic GCs, more than twice that of $B-V$ and easily converted to $[\text{Fe}/\text{H}]$ metallicities on the Zinn (1985) scale with a mean standard deviation of 0.19 dex (cf. Harris & Harris 2002). However, Figure 8c suggests that even the color-metallicity transformation relation using $C-T_1$ is subject to large uncertainty in metallicity estimation, if there are sizable age differences amongst GCs within and between galaxies.

3.2. Comparison with Globular Cluster Systems in M31, M87, and NGC 1399

We have demonstrated in § 3.1 that detailed modeling of HB morphology is important in stellar population synthesis by calibrating our models using the sample of Galactic GCs. We now compare data from the M31, M87, and NGC 1399 GC systems with our models in order to investigate whether they show any systematic differences, particularly in terms of age, compared with their Galactic counterparts. In Paper I we suggested that the GC systems of M87 and NGC 1399 are a few billion years older than the Milky Way system,

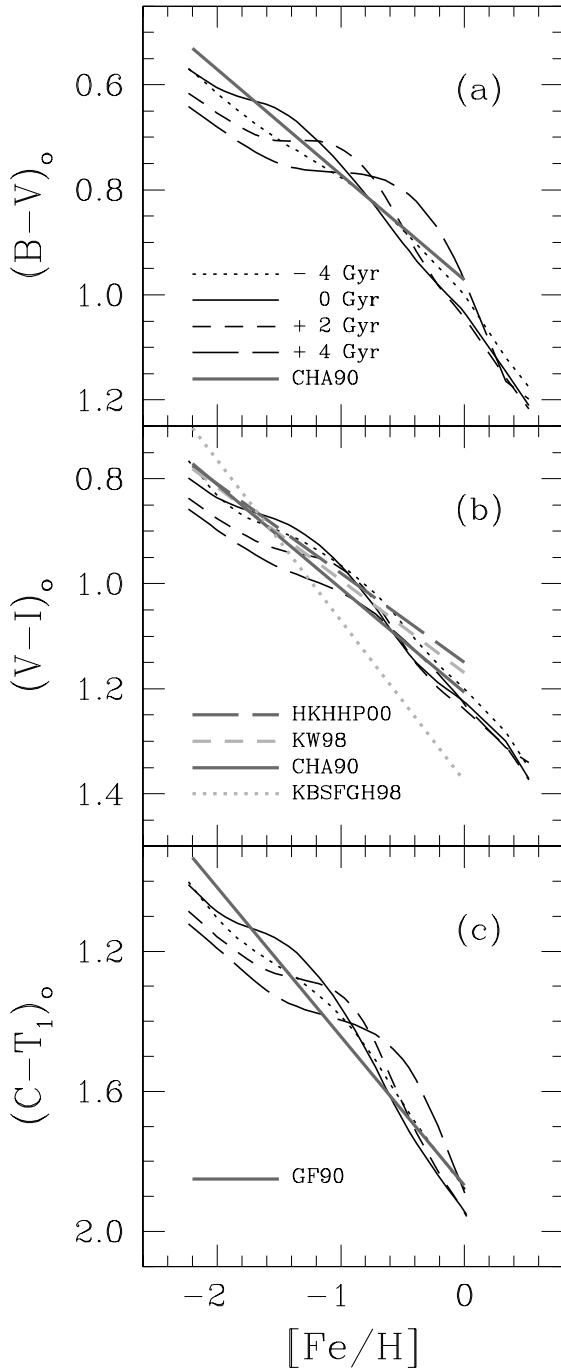


FIG. 8.—Our models contrasted with several *linear* color-metallicity transformation relations. Symbols for our models are shown in (a). In the $[\text{Fe}/\text{H}]$ vs. $(B-V)_0$ plane (a), CHA90's relation (gray solid line), in the $[\text{Fe}/\text{H}]$ vs. $(V-I)_0$ plane (b), CHA90's relation (gray solid line), KBSFGH98's relation (gray dotted line), KW98's relation (gray short-dashed line), and HKHHP00's relation (gray long-dashed line), and in the $[\text{Fe}/\text{H}]$ vs. $(C-T_1)_0$ plane (c), GF90's relation (gray solid line) are compared, respectively, with our models (see text).

based upon an analysis of the $[\text{Fe}/\text{H}]$ versus $H\beta$ plane. We now examine this claim using integrated broadband colors instead of $H\beta$.

For the M31 system we use the Barmby et al. (2000) compilation. As in the case of the Galactic GC system we restrict the M31 sample to those with $E(B-V) < 0.2$ and $\sigma[\text{Fe}/\text{H}] < 0.2$. Figure 9 compares the M31 GCs (filled

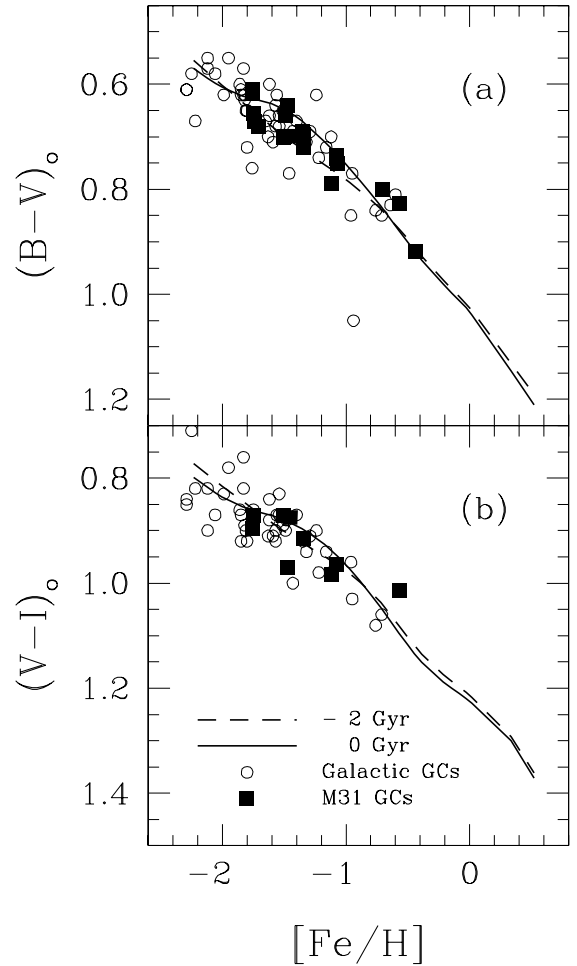


FIG. 9.—M31 GCs (filled squares; $E(B-V) < 0.2$, $\sigma[\text{Fe}/\text{H}] < 0.2$, data from Barmby et al. 2000) compared with our models in the (a) $(B-V)_0$ and (b) $(V-I)_0$ vs. $[\text{Fe}/\text{H}]$ planes. For comparison, Galactic GCs (open circles; $E(B-V) < 0.2$) are also plotted. Note that our models reproduce the observational data reasonably well and there are no significant differences between the Galactic and M31 systems.

squares) with our models in the (a) $(B-V)_0$ and (b) $(V-I)_0$ versus $[\text{Fe}/\text{H}]$ planes; Galactic GCs with $E(B-V) < 0.2$ (open circles) are also plotted. The M31 GCs are reasonably well reproduced by our models, and we suggest that there are no significant differences between the Galactic and M31 systems.

For the case of the M87 GC system there are at least two photometric studies carried out in the $UBVRI$ system (Strom et al. 1981, hereafter SFHSWS81; CHA90). Both data sets, however, suffer to some degree from uncertain photometric accuracy. These data, after being combined with Cohen et al.'s (1998) spectroscopic metallicity determinations, are compared with our models in Figure 10. We adopt a foreground reddening of $E(B-V) = 0.02$ (Burstein & Heiles 1982), corresponding to $E(C-T_1) = 0.04$.

A comparison of the SFHSWS81 photometry for the M87 GC system with our models is shown in Figures 10a ($U-B)_0$, (b) $(U-R)_0$, and (c) $(B-R)_0$. Here the brighter sample of data ($B < 21$) is highlighted with large filled circles, while the fainter sample ($B < 22$) is shown with small open circles. SFHSWS81 suggest that uncertainties in their color zero points amount to 0.1–0.2 mag. We found that zero-point offsets of 0.08 mag in $U-B$, 0.11 mag in $U-R$, and

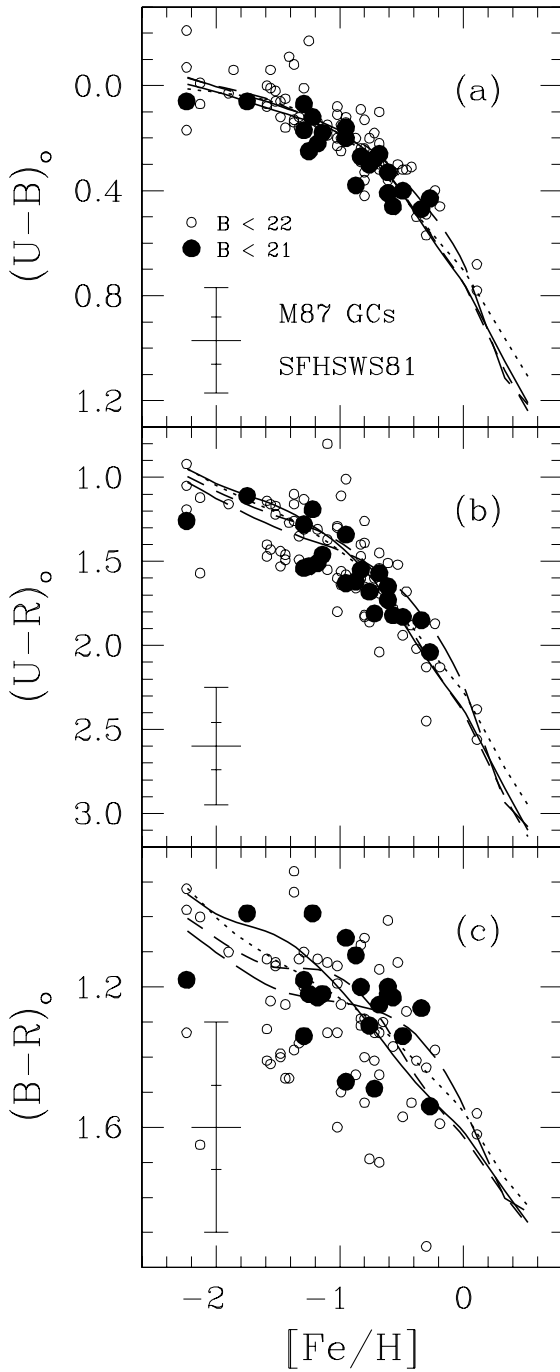


FIG. 10.—M87 GCs (small open circles; $B < 22$, large filled circles; $B < 21$, photometric data from SFHSWS81, $[\text{Fe}/\text{H}]$ from Cohen et al. 1998) compared with our models in the (a) $(U-B)_0$, (b) $(U-R)_0$, and (c) $(B-R)_0$ vs. $[\text{Fe}/\text{H}]$ planes. Symbols for our models are same as in Fig. 2. Photometric errors are displayed for clusters with $B < 21$ (small error bars) and with $B < 22$ (large error bars), respectively. Note that our models are consistent with the data, though it is difficult to extract robust age information from this sample because of the still large observational errors (see text).

0.01 mag in $B-R$ were necessary to match our models to their photographic photometry. The models are consistent with the data, particularly for the brighter clusters with smaller observational uncertainties. Although it is difficult to extract robust age information from this sample, Figure 10c nevertheless shows that higher quality data particularly

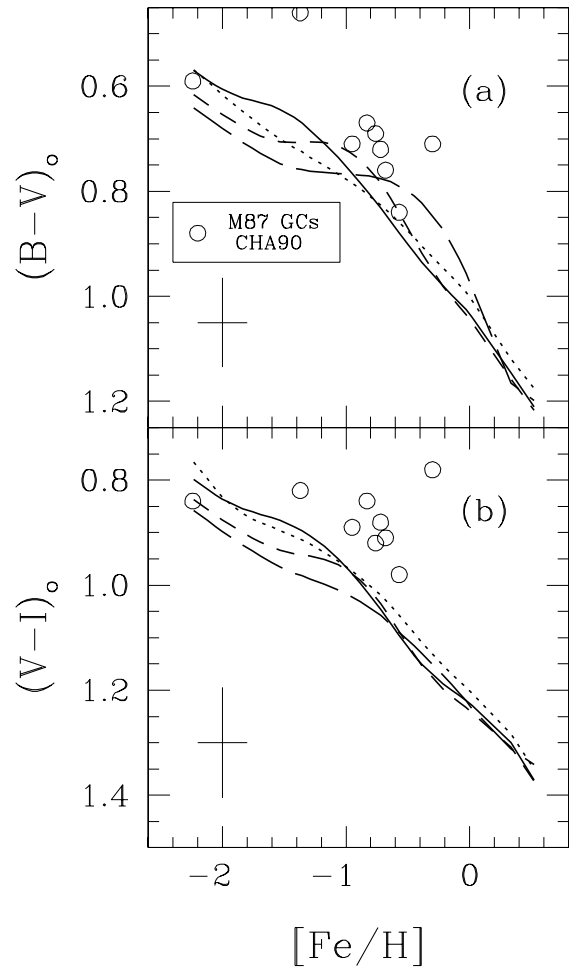


FIG. 11.—M87 GCs (photometric data from CHA90, $[\text{Fe}/\text{H}]$ from Cohen et al. 1998) compared with our models in the (a) $(B-V)_0$ and (b) $(V-I)_0$ vs. $[\text{Fe}/\text{H}]$ planes. Symbols for our models are same as in Fig. 2. Note that there seem to be systematic zero-point offsets (see text).

in the regime of $[\text{Fe}/\text{H}] < -1$ may allow for a useful age discrimination in the future.

Another comparison of M87 GCs (using photometric data from CHA90) with our models in the $(B-V)_0$ and $(V-I)_0$ versus $[\text{Fe}/\text{H}]$ planes is presented in Figure 11. It appears that this sample of M87 GCs also exhibits systematic zero-point offsets, as noted by Couture et al., of the order of ± 0.04 mag in color. With only nine clusters in common between CHA90 and Cohen et al. (1998) it is difficult to obtain useful age information of this system, mainly because of the residual observational uncertainties. Additional high-quality photometric data (at least B , V , and I) are urgently required in order to examine any potential age differences between GC systems in M87 and the Milky Way.

The Washington CCD photometry for the M87 GCs is compared with our models in Figure 12. Thirty-two clusters have both photometry (LG93) and spectroscopy (Cohen et al. 1998). We have used only 25 of these here, excluding the C field (photometric uncertainty) and W field (nonphotometric night) data of LG93; they are plotted in Figures 12a and 12b. The typical photometric error in $C-T_1$ for the cluster sample is 0.06 mag, but it is far smaller for the brighter GCs. The typical uncertainty in spectroscopic metallicity is ~ 0.2 dex and, for purposes of clarity, is not displayed here.

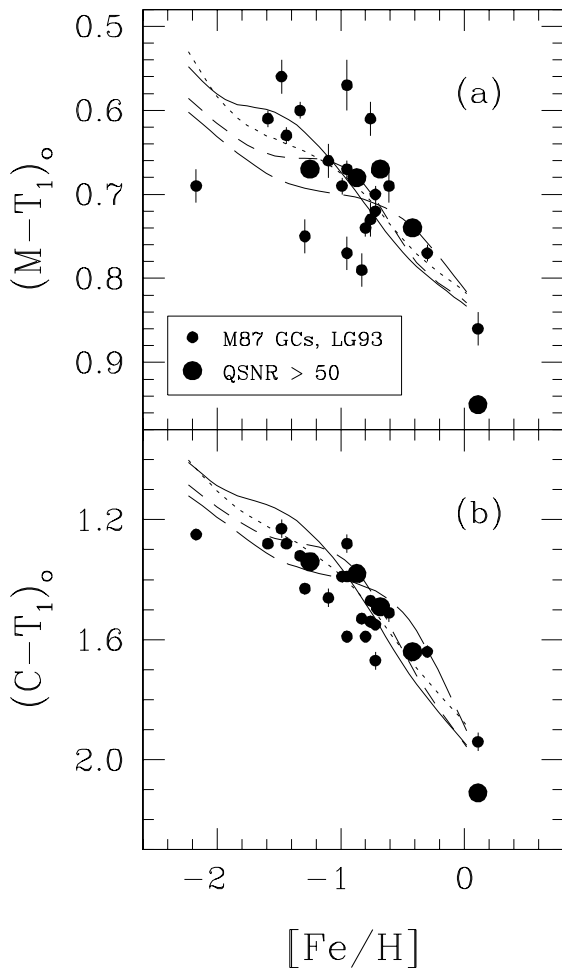


FIG. 12.—M87 GCs (photometric data from LG93, $[\text{Fe}/\text{H}]$ from Cohen et al. 1998; *large symbols*, $QSNR > 50$) compared with our models in the (a) $(M-T_1)_0$ and (b) $(C-T_1)_0$ vs. $[\text{Fe}/\text{H}]$ planes. Symbols for our models are same as in Fig. 2. Note that our models trace the data reasonably well, although the low quality of the M87 GCs photometry prevents us from any precise age estimation.

The $QSNR$, defined by Cohen et al. (1998) in their spectroscopic analysis, correlates with photometric magnitude in the sense that brighter clusters are of higher $QSNR$. The large filled circles of Figure 12 have $QSNR > 50$ and are the relatively bright clusters with relatively high accuracy in photometry as well as in spectroscopy. It is seen from Figure 12 that, even though our models trace the data reasonably well, the low quality of the M87 GCs photometry prevents us from any precise age estimation.

In Figure 13 we present a comparison of the NGC 1399 GCs (photometric data from Kissler-Patig et al. 1997; $[\text{Fe}/\text{H}]$ from KBSFGH98) with our models in the $[\text{Fe}/\text{H}]$ versus $(V-I)_0$ plane. There appears to be a systematic offset between the data and our models. KBSFGH98's color-metallicity transformation relation (Fig. 8b) differs substantially from other comparable relations; therefore, it would be worthwhile to get more high-quality photometry of metal-rich clusters to address this seeming discrepancy.

3.3. UV Photometry

We can conclude from § 3.2 that reliable age information for extragalactic GC systems is difficult to obtain with the

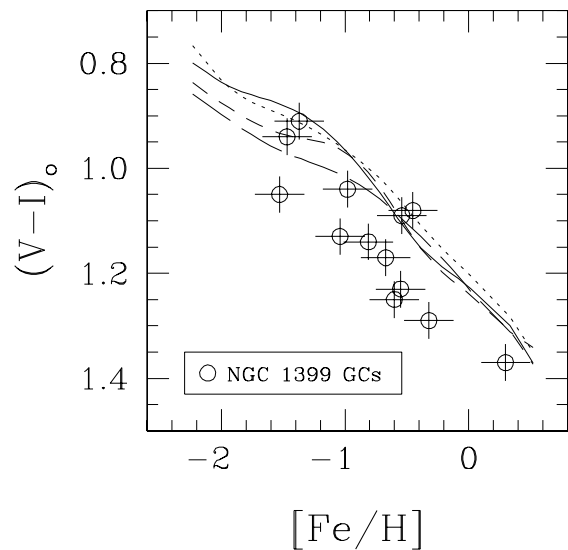


FIG. 13.—NGC 1399 GCs (photometric data from Kissler-Patig et al. 1997; $[\text{Fe}/\text{H}]$ from KBSFGH98) compared with our models in the $[\text{Fe}/\text{H}]$ vs. $(V-I)_0$ plane. Symbols for our models are same as in Fig. 2. It appears that there is a systematic offset between the data and our models.

currently available optical to near-IR data. As suggested in § 2.3, however, far-UV photometry would appear to be more useful as an age discriminant. Here we examine whether our theoretical UV to optical colors can be applied to the available UV photometry of globular clusters in the Milky Way and M31.

In Figure 14 data for the Galactic GCs from the *Orbiting Astronomical Observatory* (*OAO 2*, filled circles) and the *Astronomical Netherlands Satellite* (*ANS*, filled squares) and those for the M31 GCs from the *Ultraviolet Imaging Telescope* (*UIT*, open circles) are plotted with our models. Triangles represent the relatively highly reddened clusters with $E(B-V) > 0.2$. For the Galactic system there are seven far-UV and 13 near-UV data points from the *OAO 2* and 17 far-UV and 22 near-UV data points from the *ANS* (Dorman, O'Connell, & Rood 1995). Bohlin et al. (1993) report 43 near-UV and four far-UV detections of M31 GCs using the *UIT*. From their Tables 2 and 3, however, photometry is used here from only 17 near-UV and zero far-UV observations, after the exclusion of uncertain identifications (indicated by a colon following the Bo identification in their tables) and considering only those with both $[\text{Fe}/\text{H}]$ and $E(B-V)$ from Barmby et al. (2000).

The predicted $(15-V)_0$ colors from our models as a function of $[\text{Fe}/\text{H}]$ are compared with Galactic GCs in the left panels of Figure 14. The *OAO 2* photometry is shown in Figure 14a, and Figure 14b presents that from the *ANS*. The errors associated with the *OAO 2* data amount to ~ 0.5 mag, and they are omitted in Figure 14a. As we compare the observations with Figure 1, we note that they fall within the suggested age range of our model predictions. Moreover, the far-UV flux from the well-known second parameter pair M3 and M13 (*crosses*) is explicable with a relative age difference of ~ 1.5 Gyr between the pair. This is consistent with the recent age estimation for these clusters based on their optical CCD photometry (Rey et al. 2001). We also note that 47 Tuc (Fig. 14a) is well reproduced by our models, verifying our estimation of the PAGB star contribution to the

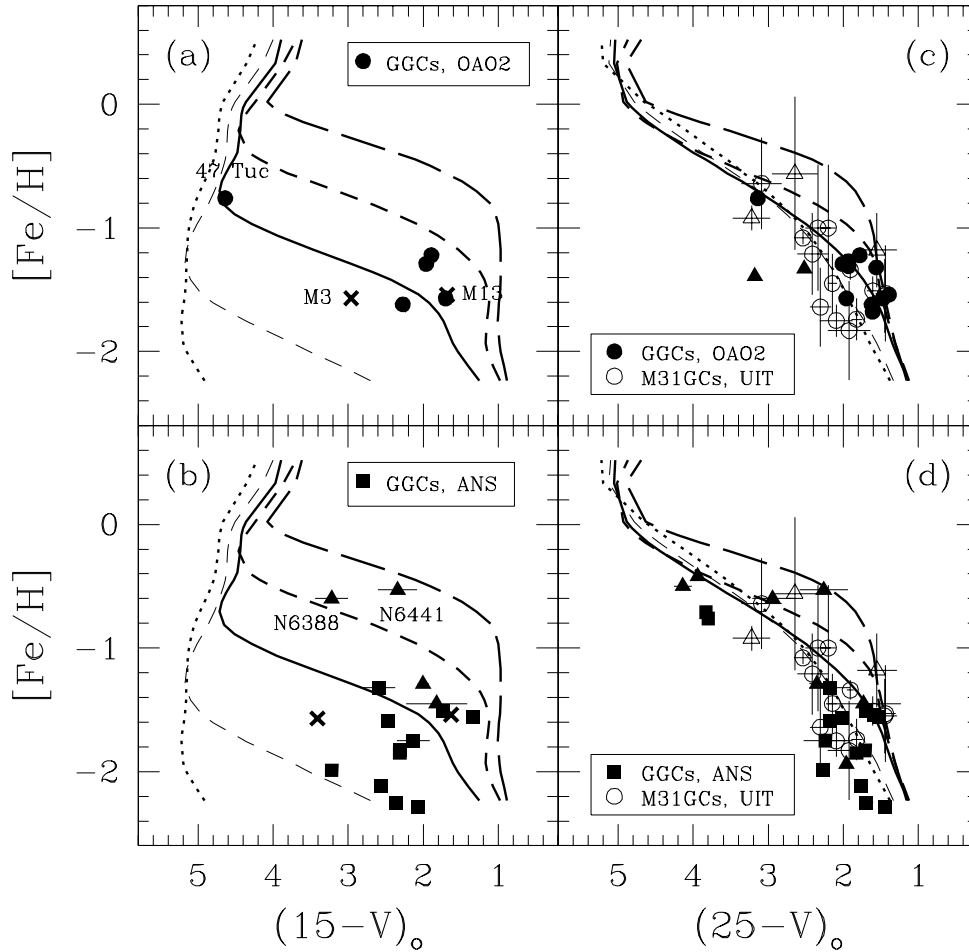


FIG. 14.—Available UV photometry of Galactic and M31 GCs compared with our models in the $(15-V)_0$ vs. $[\text{Fe}/\text{H}]$ (*a* and *b*) and in the $(25-V)_0$ vs. $[\text{Fe}/\text{H}]$ (*c* and *d*) planes. Symbols for our models are same as in Fig. 6. The Galactic GCs obtained from *OAO 2* are indicated as filled circles and those from *ANS* are indicated as filled squares, respectively. The second-parameter Galactic GCs, M3, and M13, are depicted as crosses in the left panels. The M31 GCs observed from *UIT* are indicated as open circles. Triangles are the data with $E(B-V) > 0.2$. The Galactic GCs' UV photometric data and $[\text{Fe}/\text{H}]$ are from Dorman et al. (1995) and Harris (1996), respectively, and those of M31 GCs are from Bohlin et al. (1993) and Barmby et al. (2000), respectively. Note that the observations fall within the suggested age range of our model predictions (see text).

integrated far-UV flux. The use of far-UV to optical colors is, therefore, suggested as the most promising chronometer for GC systems, with the admitted caveat that there are a few peculiar GCs, such as NGC 6388 and NGC 6441, with unexpected extended blue HB stars (Rich et al. 1997). If there are significant age differences between Milky Way and giant elliptical GC systems, in the sense of the latter being 2–3 Gyr older (as suggested in Paper I), then we predict that the majority of metal-rich clusters would be far-UV bright compared with Galactic counterparts. In this respect the results from the recent *HST* far-UV photometry of GC systems in Virgo ellipticals (GO 8643 and GO 8725) are highly anticipated.

In the right panels of Figure 14 the $(25-V)_0$ colors of M31 GCs (*UIT* data, *open circles*) are shown with our models as a function of $[\text{Fe}/\text{H}]$. In addition, the relevant data for Galactic GCs (*OAO 2*, Fig. 14*c*; *ANS*, Fig. 14*d*) are overplotted for comparison. We have recalibrated the $(25-V)_0$ colors of the M31 GCs by adopting V and $E(B-V)$ from Barmby et al. (2000). Our models represent the near-UV photometry of M31 GCs, as well as those in the Milky Way, with no significant differences seen between the two systems, especially when disregarding the highly reddened clusters

(*triangles*). This again suggests that the M31 and Milky Way GC systems are fundamentally similar, in agreement with the analysis of optical to near-IR colors seen in § 3.2, and it is consistent with the earlier conclusions of Bohlin et al. (1993). As discussed in § 2.3, it is somewhat difficult to discriminate age differences of GC systems using the near-UV photometry alone. Far-UV photometry of the M31 GCs would be highly desirable to better quantify our findings. In this respect a large UV photometry data set for the M31 GC system from the upcoming *GALEX*⁹ mission will become an invaluable resource.

4. CONCLUSIONS AND DISCUSSION

The primary goal of our paper is to investigate the effects of horizontal-branch stars on the integrated broadband colors of old, simple stellar populations. To do so, we have employed a unique, self-consistent treatment of HB morphology as a function of age and metallicity. We have found that some temperature-sensitive integrated broadband

⁹ At <http://www.srl.caltech.edu/galex>.

colors are significantly affected by the presence of blue HB stars within our investigated age range of $-4 \text{ Gyr} \leq \Delta t \leq +4 \text{ Gyr}$ (i.e., $8 \text{ Gyr} \leq t \leq 16 \text{ Gyr}$). The close agreement between our models and the relatively low-reddened inner halo Galactic GCs in both the Johnson-Cousins and Washington filter systems is encouraging. The use of far-UV to optical colors is suggested to be a powerful age-dating regime for old stellar systems when coupled with realistic HB morphologies (Lee 2001a, 2001b). Future observations of GC systems in external galaxies from large ground-based telescopes and space UV facilities will enable us to quantify any systematic age differences between the various systems. A more sophisticated understanding of the theory governing mass loss and helium enrichment will also contribute to a better understanding of stellar age determination using far-UV photometry (O'Connell 1999).

In the case of the M31 GC system our work suggests that it is not fundamentally different from the Galactic system, from the UV through to the near-IR. This is in contrast to several studies that have claimed that the metal-rich M31 GCs could be much younger than the metal-poor sample (e.g., Burstein et al. 1984; Barmby & Huchra 2000). Future far-UV data sets to be provided, for example, by the *GALEX* mission should aid in resolving this controversy. Further Washington system photometry will also be valuable (Lee et al. 2001).

The study of extragalactic GC systems today is being driven primarily by an attempt to understand the bimodal color distributions seen from many early-type galaxies (e.g., Larsen et al. 2001; Kundu & Whitmore 2001), as well as from some spirals (Forbes, Brodie, & Larsen 2001b). The

origin of these blue and red subpopulations and the implications for the formation of their host galaxies remains unclear. If a relative age difference exists between the subpopulations, an important piece of the galaxy formation puzzle will have been found. Identifying useful age discriminants remains an important component of cosmology and galaxy formation. The broadband photometric predictions described here, in combination with the spectroscopic discriminants of Paper I, should provide observers with the necessary tools to discriminate age differences among GC subpopulations. Finally, we conclude that several of the canonical *linear* color-metallicity transformation relations should be used with caution if there are sizable age differences among globular clusters within and between galaxies. It remains to be seen whether bimodal color distributions can be interpreted as simple metallicity or age differences, or whether a more complicated interplay between metallicity and age must be involved.

It is a pleasure to thank P. Barmby for M31 GCs data, M. G. Lee for M87 GCs data, T. Lejeune for his updated color table, and S. K. Yi for many helpful discussions. We are also grateful to the anonymous referee for her/his detailed report, which helped us improve this paper. Support for this work was provided by the Creative Research Initiatives Program of the Korean Ministry of Science and Technology. This work was also supported by the Postdoctoral Fellowship Program of the Korea Science and Engineering Foundation. B. K. G. acknowledges the support of the Australian Research Council through its Large Research Grant Program (A00105171).

REFERENCES

- Ashman, K. M., & Zepf, S. E. 1998, *Globular Cluster Systems* (Cambridge: Cambridge Univ. Press)
- Barmby, P., & Huchra, J. P. 2000, *ApJ*, 531, L29
- Barmby, P., Huchra, J. P., Brodie, J. P., Forbes, D. A., Schroder, L. L., & Grillmair, C. J. 2000, *AJ*, 119, 727
- Bohlin, R. C., et al. 1993, *ApJ*, 417, 127
- Brocato, E., Castellani, V., Poli, F. M., & Raimondo, G. 2000, *A&AS*, 146, 91 (BCPR00)
- Bruzual, G., & Charlot, S. 1993, *ApJ*, 405, 538
- Burstein, D., Faber, S. M., Gaskell, C. M., & Krumm, N. 1984, *ApJ*, 287, 586
- Burstein, D., & Heiles, C. 1982, *AJ*, 87, 1165
- Buzzoni, A. 1989, *ApJS*, 71, 817
- . 1995, *ApJS*, 98, 69
- Canterna, R. 1976, *AJ*, 81, 228
- Cardelli, J. A., Clayton, G. C., & Mathis, J. S. 1989, *ApJ*, 345, 245
- Cellone, S. A., & Forte, J. C. 1996, *ApJ*, 461, 176 (CF96)
- Chaboyer, B., Demarque, P., Kernan, P. J., & Krauss, L. M. 1998, *ApJ*, 494, 96
- Cohen, J. G., Blakeslee, J. P., & Ryzhov, A. 1998, *ApJ*, 496, 808
- Couture, J., Harris, W. E., & Allwright, J. W. B. 1990, *ApJS*, 73, 671 (CHA90)
- Demarque, P., Chaboyer, B., Guenther, D., Pinsonneault, M., & Yi, S. 1996, *Yale Isochrones* (New Haven: Yale Univ. Obs.)
- Dinescu, D. I., Girard, T. M., & van Altena, W. F. 1999, *AJ*, 117, 1792
- Dorman, B., O'Connell, R. W., & Rood, R. T. 1995, *ApJ*, 442, 105
- Forbes, D. A., Beasley, M. A., Brodie, J. P., & Kissler-Patig, M. 2001a, *ApJ*, 563, L143
- Forbes, D. A., Brodie, J. P., & Larsen, S. 2001b, *ApJ*, 556, L83
- Geisler, D., & Forte, J. C. 1990, *ApJ*, 350, L5 (GF90)
- Geisler, D., Lee, M. G., & Kim, E. 1996, *AJ*, 111, 1529
- Gibson, B. K., Madgwick, D. S., Jones, L. A., Da Costa, G. S., & Norris, J. E. 1999, *AJ*, 118, 1268
- Girardi, L. 2001, in *IAU Symp. 207, Extragalactic Star Clusters*, ed. E. K. Grebel, D. Geisler, & D. Minniti, in press (astro-ph/0108198)
- Girardi, L., Bressan, A., Bertelli, G., & Chiosi, C. 2000, *A&AS*, 141, 371
- Hansen, B. M. S., et al. 2002, *ApJ*, 574, L155
- Harris, G. L. H., Geisler, D., Harris, H. C., & Hesser, J. E. 1992, *AJ*, 104, 613
- Harris, H. C., & Canterna, R. 1977, *AJ*, 82, 798
- Harris, W. E. 1996, *AJ*, 112, 1487
- Harris, W. E., & Harris, G. L. H. 2002, *AJ*, 123, 3108
- Harris, W. E., Harris, G. L. H., & McLaughlin, D. E. 1998, *AJ*, 115, 1801
- Harris, W. E., Kavelaars, J. J., Hanes, D. A., Hesser, J. E., & Pritchett, C. J. 2000, *ApJ*, 533, 137 (HKHHP00)
- Kissler-Patig, M., Brodie, J. P., Schroder, L. L., Forbes, D. A., Grillmair, C. J., & Huchra, J. P. 1998, *AJ*, 115, 105 (KBSFGH98)
- Kissler-Patig, M., Kohle, S., Hilker, M., Richtler, T., Infante, L., & Quintana, H. 1997, *A&A*, 319, 470
- Kundu, A., & Whitmore, B. C. 1998, *AJ*, 116, 2841 (KW98)
- . 2001, *AJ*, 121, 2950
- Kurth, O. M., Fritze-von Alvensleben, U., Fricke, K. J. 1999, *A&AS*, 138, 19 (KFF99)
- Kurucz, R. L. 2001, astro-ph/0105400
- Larsen, S. S., Brodie, J. P., Huchra, J. P., Forbes, D. A., & Grillmair, C. 2001, *AJ*, 121, 2974
- Lee, H.-c. 2001a, Ph.D. thesis, Yonsei Univ.
- . 2001b, *PASP*, 113, 1021
- Lee, H.-c., Yoon, S.-J., & Lee, Y.-W. 2000, *AJ*, 120, 998 (Paper I)
- Lee, M. G., & Geisler, D. 1993, *AJ*, 106, 423 (LG93)
- Lee, M. G., Kim, S. C., Geisler, D., Seguel, J., Sarajedini, A., & Harris, W. 2001, in *IAU Symp. 207, Extragalactic Star Clusters*, ed. E. K. Grebel, D. Geisler, & D. Minniti, in press (astro-ph/0109219)
- Lee, Y.-W., Demarque, P., & Zinn, R. 1994, *ApJ*, 423, 248
- Lejeune, T., & Buser, R. 1996, *Baltic Astron.*, 5, 399
- Lejeune, T., Cuisinier, F., & Buser, R. 1997, *A&AS*, 125, 229
- . 1998, *A&AS*, 130, 65
- Maraston, C. 1998, *MNRAS*, 300, 872
- O'Connell, R. W. 1999, *ARA&A*, 37, 603
- Ostrov, P. G., Forte, J. C., & Geisler, D. 1998, *AJ*, 116, 2854
- Recio-Blanco, A., Piotto, G., Aparicio, A., & Renzini, A. 2002, *ApJ*, 572, L71
- Reimers, D. 1975, *Mem. Soc. R. Sci. Liège*, 8, 369
- Rey, S.-C., Yoon, S.-J., Lee, Y.-W., Chaboyer, B., & Sarajedini, A. 2001, *AJ*, 122, 3219
- Rich, R. M., et al. 1997, *ApJ*, 484, L25
- Salaris, M., Chieffi, A., & Straniero, O. 1993, *ApJ*, 414, 580
- Salaris, M., & Weiss, A. 2002, *A&A*, 388, 492
- Salpeter, E. E. 1955, *ApJ*, 121, 161
- Sarajedini, A., Chaboyer, B., & Demarque, P. 1997, *PASP*, 109, 1321

- Schönberner, D. 1983, *ApJ*, 272, 708
- Secker, J., Geisler, D., McLaughlin, D. E., & Harris, W. E. 1995, *AJ*, 109, 1019
- Strom, S. E., Forte, J. C., Harris, W. E., Strom, K. M., Wells, D. C., & Smith, M. G. 1981, *ApJ*, 245, 416 (SFHSWS81)
- Vazdekis, A., Casuso, E., Peletier, R. F., & Beckman, J. E. 1996, *ApJS*, 106, 307
- Westera, P., Lejeune, T., Buser, R., Cuisinier, F., & Bruzual, G. 2002, *A&A*, 381, 524
- Wheeler, J. C., Sneden, C., & Truran, J. W., Jr. 1989, *ARA&A*, 27, 279
- Worthey, G. 1994, *ApJS*, 95, 107 (W94)
- Yi, S., Demarque, P., & Kim, Y.-C. 1997, *ApJ*, 482, 677
- Yi, S., Demarque, P., Kim, Y.-C., Lee, Y.-W., Ree, C. H., Lejeune, T., & Barnes, S. 2001, *ApJS*, 136, 417
- Yi, S., Lee, Y.-W., Woo, J.-H., Park, J.-H., Demarque, P., & Oemler, A., Jr. 1999, *ApJ*, 513, 128
- Zepf, S. E., Ashman, K. M., & Geisler, D. 1995, *ApJ*, 443, 570
- Zinn, R. 1985, *ApJ*, 293, 424